Bulk modulational instability in photonic topological insulators

Aleksandra Maluckov,[1,2] Daniel Leykam,[1,3] and et al.

[1] *Center for Theoretical Physics of Complex Systems, Institute for Basic Science, Daejeon 34126, Korea*
[2] *P* Group, Vinča Institute of Nuclear Sciences, University of Belgrade, P.O. Box 522, 11001 Belgrade, Serbia*
[3] *Basic Science Program, Korea University of Science and Technology, Daejeon 34113, Korea*

(Dated: June 25, 2020)

We study modulational instability of Bloch waves in nonlinear Chern insulators, showing that the instability dynamics are sensitive to the Bloch band's topology. At short times, captured by the linear stability analysis, the nonlinear Bloch waves exhibit long wavelength instabilities for both the self-focusing and self-defocusing nonlinearity, and a re-emergence of stability at a critical Bloch wave intensity, corresponding to the bifurcation of a nonlinear Dirac cone. At longer times, nonlinear wave mixing processes result in an energy-selective excitation of the modes of the initially-excited band, enabling direct measurement of its Chern number via the Fourier spectrum of the wave field. Interestingly this coincides with a pre-thermalization regime in which the topological observables reach a steady state, although an effective thermal equilibrium has not yet been established. Our analytical and numerical results establish modulational instability dynamics as a tool to probe the bulk topology of bosonic lattices and create topologically nontrivial wave fields.

Topologically nontrivial photonic bands can be combined with appreciable mean-field nonlinear interactions in a variety of experimental platforms [1–3], including exciton-polariton condensates in structured microcavities [4, 5], nonlinear waveguide arrays [6], metasurfaces [7], and ring resonators [8, 9]. These nonlinear topological photonic systems are of growing interest not only due to their ability to host novel phenomena with no analogue in electronic topological materials, but also due to their potential device applications such as novel types of lasers, optical isolators, and frequency combs. Existing theoretical studies have focused on the use of nonlinearities to control the propagation of wavepackets accessible in the linear limit, such as the self-focusing of unidirectional edge states [10–13], the formation of self-localized modes in the bulk of topological lattices [14–16], or nonlinearity-induced coupling between bulk and edge states [17]. As complex nonlinear wave systems are typically sensitive to perturbations, precise control over excitation conditions is required. The robustness of these effects to disorder remains an open question, potentially limiting their utility.

In this paper we demonstrate that the nonlinear dynamics of Bloch waves in topological bands can be sensitive to the Chern number. Moreover, we show that modulational instability can lead to the *spontaneous* formation of wave *fields* characterized by non-trivial Chern numbers inherited from the linear Bloch bands. The underlying mechanism is the energy-dependent parametric gain provided by the modulational instability [18–23], which enables selective population of a single Bloch band starting from a simple plane wave initial state. In addition to providing a mechanism for sculpturing novel structured light fields, the modulational instability provides a simple way to measure the bulk topological invariants of bosonic wave systems. This is generally a difficult task unless the corresponing eigenstates *a priori* are known, the time-consuming Bloch band /Berry curvature tomography [24–27] is performed, or the bulk-edge correspondence [28–30] is considered. Moreover, our approach is based on the generic phenomenon of modulational instability and insensitive to the precise form of the nonlinearity and its sign (i.e., whether the interactions are self-focusing or defocusing).

We consider the modulational instability of nonlinear Bloch waves, employing the linear stability analysis to characterize the dynamics at short propagation times and direct numerical simulations to establish the formation of a quasi-equilibrium wave field at long times. At low intensities the instability remains confined to the initially-excited band, with nonlinear wave mixing processes leading to the excitation of all band's linear modes [31–34]. Consequently, the band's Chern number is imprinted on the Fourier spectrum of the wave field [35, 36]. Interestingly, this quasi-equilibrium state emerges well before the system is able to thermalize. At higher intensities strong interband mixing prevents the formation of a quasi-equilibrium state described by a time-independent Chern number. However the instability spectrum itself becomes sensitive to the topological properties of the band, exhibiting a re-emergence of stability at a critical intensity associated with the bifurcation of a nonlinear Dirac cone [37]. Thus, the topological properties of the band can effect the modulational instability at both small and large time and intensity scales.

We begin with the two-dimensional nonlinear Schrödinger equation describing the nonlinear (mean-field) wave propagation dynamics in photonic lattices,

$$i\partial_t \left|\psi(\boldsymbol{r})\right\rangle = (\hat{H}_L + \hat{H}_{NL}) \left|\psi(\boldsymbol{r})\right\rangle, \tag{1}$$

where $\hat{H}_L$ and $\hat{H}_{NL}$ are linear and nonlinear parts of the Hamiltonian, respectively, and $\boldsymbol{r} = (x, y)$ indexes the lattice sites. We take $\hat{H}_L$ to correspond to the chiral-π-

flux model illustrated in Fig. 1(a) [38], a two band tight binding model for a Chern insulator on a square lattice with two sublattices a and b, i.e. $|\psi(\boldsymbol{r})\rangle = (\psi_a, \psi_b)^T$, described by the Bloch wave Hamiltonian

$$\hat{H}_L(\mathbf{k}) = \boldsymbol{d}(\boldsymbol{k}) \cdot \hat{\boldsymbol{\sigma}}, \quad d_z = \Delta + 2J_2(\cos k_x - \cos k_y) \tag{2}$$
$$d_x + id_y = J_1[e^{-i\pi/4}(1 + e^{i(k_y - k_x)}) + e^{i\pi/4}(e^{-ik_x} + e^{ik_y})],$$

where $\boldsymbol{k} = (k_x, k_y)$ is the wavevector, restricted to the first Brillouin zone $k_{x,y} \in [-\pi, \pi]$, $\hat{\boldsymbol{\sigma}} = (\hat{\sigma}_x, \hat{\sigma}_y, \hat{\sigma}_z)$ are Pauli matrices, $J_{1,2}$ are nearest and next-nearest neighbour hopping strengths, and Δ is a detuning between the sublattices.

The Bloch wave eigenstates of Eq. (2) form two bands, $\hat{H}_L(\boldsymbol{k})\,|u_\pm(\boldsymbol{k})\rangle = E_\pm(\boldsymbol{k})\,|u_\pm(\boldsymbol{k})\rangle$. Fig. 1(b) shows the energy spectrum $E_\pm(\boldsymbol{k})$, which exhibits a topological phase transition at the gap closing point $\Delta/J_1 = \pm 2\sqrt{2}$, corresponding to a change in the quantized Chern number [1],

$$C = \frac{1}{2\pi i}\int_{BZ} \mathcal{F}(\boldsymbol{k}), \tag{3}$$

where $\mathcal{F}(\boldsymbol{k})$ is the Berry curvature. In a two band system the Berry curvature can be expressed in terms of the wave polarization field $\hat{\boldsymbol{n}}(\boldsymbol{k}) = \langle u_\pm(\boldsymbol{k})|\,\hat{\boldsymbol{\sigma}}\,|u_\pm(\boldsymbol{k})\rangle$, i.e.

$$\mathcal{F}(\boldsymbol{k}) = -\frac{1}{2}\hat{\boldsymbol{n}} \cdot [(\partial_{k_x}\hat{\boldsymbol{n}}) \times (\partial_{k_y}\hat{\boldsymbol{n}})], \tag{4}$$

with the Chern number counts the number of times the polarization covers the unit sphere. We note that the interpretation of C in terms of the wave polarization field can be generalized to multi-band systems [35].

For the nonlinear part of the Hamiltonian $\hat{H}_{NL}$ we consider an on-site nonlinearity of the form

$$\hat{H}_{NL} = \Gamma \mathrm{diag}[f(|\psi_a(\boldsymbol{r})|^2), f(|\psi_b(\boldsymbol{r})|^2)], \tag{5}$$

where Γ is the nonlinear interaction strength and f is the nonlinear response function. The linear Bloch wave eigenstates of $\hat{H}_L(\boldsymbol{k})$ can be continued as nonlinear Bloch waves [39, 40], which are solutions of the nonlinear eigenvalue problem $E(\boldsymbol{k})\,|\phi(\boldsymbol{k})\rangle = (\hat{H}_L(\boldsymbol{k}) + \hat{H}_{NL})\,|\phi(\boldsymbol{k})\rangle$. To study their stability we consider small perturbations $p \ll 1$, i.e. $|\psi(\boldsymbol{r}, t)\rangle = (|\phi(\boldsymbol{k}_0)\rangle + |p(\boldsymbol{r}, t)\rangle)e^{i(\boldsymbol{k}_0 \cdot \boldsymbol{r} - Et)}$ and linearise the equations of motion Eq. (1). Perturbation modes take the form [41]

$$|p(\boldsymbol{r}, t)\rangle = |\alpha\rangle\, e^{i(\boldsymbol{k}\cdot\boldsymbol{r} + \lambda t)} + |\beta^*\rangle\, e^{-i(\boldsymbol{k}\cdot\boldsymbol{r} + \lambda^* t)}. \tag{6}$$

Modes with $\mathrm{Im}(\lambda) > 0$ are linearly unstable.

We consider the stability of the $\boldsymbol{k}_0 = (\pi, 0)$ Bloch wave $|\phi(\boldsymbol{r})\rangle = (\sqrt{I_0}, 0)^T e^{i\pi x}$, which lies at a local extremum of the band structure and persists as a nonlinear Bloch wave with energy $E_{NL} = \Delta - 4J_2 + \Gamma f(I_0)$, bifurcating from the lower band when $\Delta < 4J_2$ and from the upper band when $\Delta > 4J_2$ [see purple line in Fig. 1(b)]. While the qualitative features of the perturbation spectrum do not depend on the precise form of the nonlinear response function, to be specific we consider the case of pure Kerr nonlinearity $f(I) = I$. Fig. 1(c) plots the growth rate of the most unstable perturbation wavevector as a function of Δ and Γ. For weak nonlinearities Γ we observe behaviour qualitatively similar to the scalar nonlinear Schrödinger equation, with the band edge Bloch waves becoming unstable when the nonlinearity is self-focusing, i.e. when ($\Gamma m_{\mathrm{eff}} < 0$, where m_{eff} is the wave effective mass at $\boldsymbol{k}_0$). Mid-band nonlinear Bloch waves are unstable for weak Γ regardless of its sign. Interestingly, for stronger nonlinearities we observe a re-emergence of stability along the critical line $\Gamma I_0/2 = 4J_2 - \Delta$ [dashed line in Fig. 1(c)]. This line marks a transition from purely imaginary instability eigenvalues to pairs of complex instability eigenvalues, as shown in Fig. 1(d).

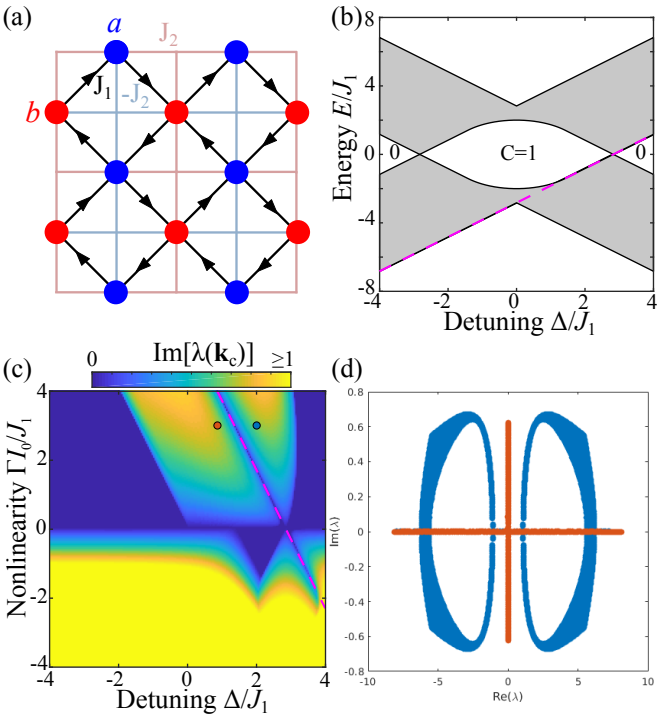

FIG. 1. Linear stability of nonlinear Bloch waves in the chiral-π-flux model. (a) Schematic of the lattice, consisting of two sublattices (a, b) with detuning Δ and inter- (intra-) sublattice couplings J_1 (J_2). (b) Linear bands (shaded regions) as a function of the sublattice detuning Δ, for $J_2 = J_1/\sqrt{2}$. (c) Growth rate of the most unstable wavevector $\boldsymbol{k}_c$ of the $\boldsymbol{k}_0 = 0$ nonlinear Bloch wave. (d) Linear stability eigenvalue spectra $\lambda(\boldsymbol{k})$ at the points indicated in (c), which are either constrained to the real and imaginary axes (brown) or form quartets of complex eigenvalues $\pm\lambda, \pm\lambda^*$ (blue).

To obtain a better understanding of this transition, we plot in Fig. 2(a) the magnitude of the most unstable wavevector, which vanishes both as $\Gamma \to 0$ and along the critical line. This suggests the instability mechanism is not specific to this particular lattice model and can be captured by a generic effective Dirac model obtained

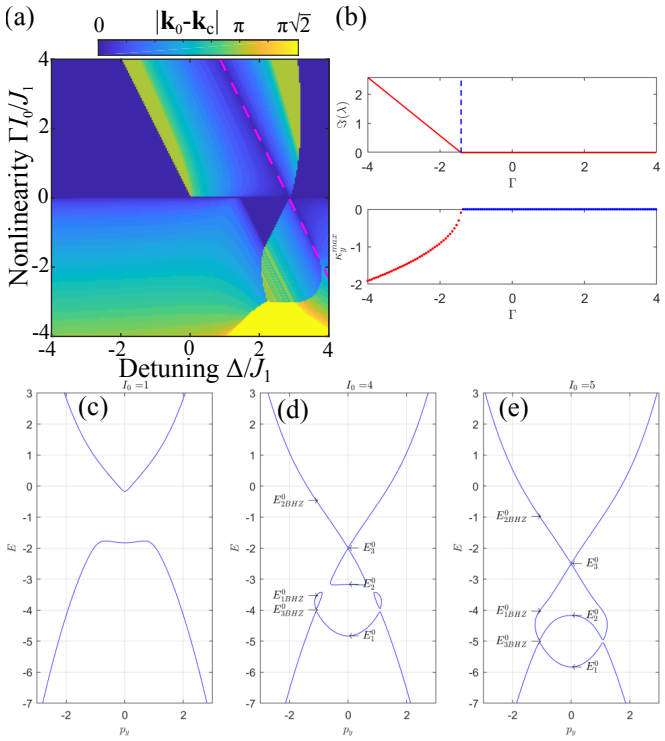

FIG. 2. (a) Magnitude of the most unstable wavevector of Fig. 1(c). (b) Cuts of the instability growth rates and wavevectors along critical lines indicated in (a). (c,d,e) The transition in the nonlinear Bloch wave spectrum across the critical line in the nontrivial (blue) and trivial (red) phases of the effective Dirac model Eq. (7). [perhaps swap panel (a) here with panel (d) of Fig. 1]

by making a long wavelength expansion of Eq. (2), i.e. $\boldsymbol{k} = \boldsymbol{k}_0 + \boldsymbol{p}$ with $\boldsymbol{p} \ll 1$,

$$\hat{H}_D = -J_1\sqrt{2}(p_x\hat{\sigma}_y + p_y\hat{\sigma}_x) + (\Delta - 4J_2 + J_2[k_x^2 + k_y^2])\hat{\sigma}_z. \tag{7}$$

Note that the quadratic $J_2[k_x^2 + k_y^2]\hat{\sigma}_z$ term is essential to correctly reproduce the Chern number $C = \frac{1}{2}(1 - \mathrm{sgn}[J_2(\Delta - 4J_2)])$ and features of the perturbation spectrum.

We can obtain the nonlinear Bloch wave solutions of Eq. (7) analytically [41], we finding that the critical line coincides with the formation of a nonlinear Dirac cone at $\boldsymbol{k}_0$ [37], i.e. a symmetry-breaking bifurcation of the nonlinear Bloch waves. Moreover, in the non-trivial phase only an additional bifurcation occurs at p_y =?, corresponding to $d_z(\boldsymbol{p}) = 0$. Due to the emergence of new solution branches at these bifurcations, all linear stability eigenvalues must vanish. Consequently, the stability of the nonlinear Bloch waves is dictated by the small $\boldsymbol{k}$ behaviour of the linear stability problem and the interplay between the energy detuning of the perturbation modes, and the nonlinearity-induced coupling between the $\boldsymbol{k}$ and $-\boldsymbol{k}$ perturbation wavevectors. The energy detuning is mainly sensitive to the sign of the nonlinearity, whereas the nonlinearity-induced coupling explicitly depends on the band topology in the continuum model Eq. (7). In the non-trivial phase the coupling is suppressed because as $\boldsymbol{k}$ increases, the perturbation mode polarization rotates away from the nonlinear Bloch wave's polarization.

The termination of the critical line in the trivial phase at $\Delta = \Delta_c = 4J_2$ is also captured by the continuum model. For $\Delta > \Delta_c$ the most unstable wavevector is $\boldsymbol{k}_c = \sqrt{J_1^2/J_2^2 + |\Gamma I_0/J_2|}$. Again, the instability is dictated by the quadratic $J_2(k_x^2 + k_y^2)$ term and vanishes in the usual linear Dirac approximation, which neglects $k_{x,y}^2$ terms. Thus, the modulational instability does not just depend on the band dispersion, but is also sensitive to the geometrical properties of the eigenstates such as the local Berry curvature. This is our first key result.

Next, we carry out numerical simulations of Eq. (1) to study the development of the instability beyond the initial linearized dynamics. We use a system size of $N = 32 \times 32$ unit cells with periodic boundary conditions [42]. To characterize the complex multi-mode dynamics, we compute the following observables of the time-dependent field: (i) The real space participation number,

$$P_{\boldsymbol{r}} = \frac{\mathcal{P}^2}{2N}\sum_{\boldsymbol{r}}\left(|\psi_a(\boldsymbol{r})|^4 + |\psi_b(\boldsymbol{r})|^4\right)^{-1}, \tag{8}$$

which measures the fraction of lattice sites strongly excited by the wave field, (ii) the Fourier space participation number $P_{\boldsymbol{k}}$, which measures similarly the fraction of excited Fourier modes, and the polarization direction $\hat{\boldsymbol{n}}(\boldsymbol{k}) = \langle\psi(\boldsymbol{k})|\,\hat{\boldsymbol{\sigma}}\,|\psi(\boldsymbol{k})\rangle\,/\,\langle\psi(\boldsymbol{k})|\psi(\boldsymbol{k})\rangle$. As we consider small random perturbations to the nonlinear Bloch wave, we average these observables over 100 different initial perturbations. The perturbation-averaged polarization $\langle\hat{\boldsymbol{n}}(\boldsymbol{k})\rangle$ in general describes a mixed state with $n^2 = \langle\hat{\boldsymbol{n}}(\boldsymbol{k})\rangle \cdot \langle\hat{\boldsymbol{n}}(\boldsymbol{k})\rangle < 1$. Nevertheless, the wave field can still be characterized by a quantized Chern number provided $n^2 > 0$ for all $\boldsymbol{k}$, i.e. the "purity gap" $\min_{\boldsymbol{k}}(n^2)$ remains open [43–45].

Fig. 3 illustrates the dynamics of the $\boldsymbol{k}_0 = (\pi, 0)$ nonlinear Bloch wave with initial intensity $I_0 = 1$, when each lattice site is subjected to a random perturbation with amplitude not exceeding $0.01\sqrt{I_0}$. We assume saturable nonlinearity of the form $f(I) = I/(1 + I)$, which takes into account the inevitable saturation of nonlinear response at high intensities. We consider parameters corresponding to three different instability regimes: imaginary self-focusing, imaginary defocusing, and complex instability. The focusing and complex instabilities generate a collection of localized solitons, resulting in a decrease in $\langle P_{\boldsymbol{r}}\rangle$ in Fig. 3(a). On the other hand, the defocusing nonlinearity spreads energy over both sublattices, resulting in a small increase in $\langle P_{\boldsymbol{r}}\rangle$. In all cases $\langle \boldsymbol{P}_{\boldsymbol{k}}\rangle$ increases due to the rest of the Brillouin zone being populated via nonlinear wave interactions. For the imaginary instabilities this is accompanied by the opening of

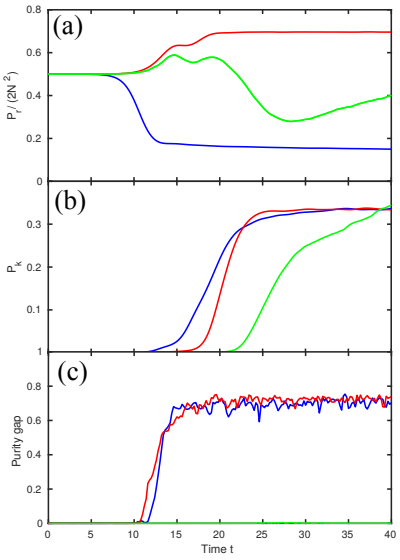

FIG. 3. Long time instability dynamics in the chiral flux π-lattice model for self-focusing ($\Delta = 0, \Gamma = -2.5$; blue), self-defocusing ($\Delta = 0, \Gamma = 5$; red), and complex ($\Delta = 2, \Gamma = 5$; green) instabilities. (a) Real space participation number. (b) Fourier space participation number. (c) Purity gap. Averages are performed over 100 realizations of initial perturbation.

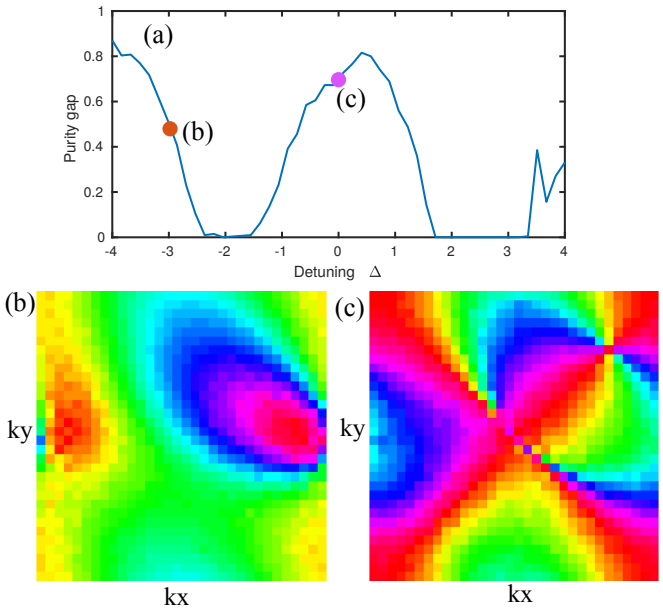

FIG. 4. (a) Purity gap time $t = t_f = 40J_1$ as a function of the detuning Δ. (b,c) Polarization textures corresponding to trivial ($\Delta = -3$, b) and non-trivial ($\Delta = 0, c$) fields at t_f. The shading denotes the in-plane (n_x, n_y), and the Chern number is obtained by summing the vortex charges weighted by $\mathrm{sgn}(n_z)$ (see Ref. [35] for details).

the purity gap and emergence of a well-defined Chern number (corresponding to the band Chern number). Interestingly we observe that the purity gap opens prior to $\langle P_{\boldsymbol{r},\boldsymbol{k}} \rangle$ reaching a steady state. In the case of the complex instability the purity gap remains negligible due to competition between pairs of instability modes with the same growth rates.

To explore the emergence of a purity gap in more detail, we present in Fig. 4(a) the value of $\min_{\boldsymbol{k}}(n^2)$ at $t = t_f = 40J_1$ as a function of the sublattice detuning Δ, which tunes the band flatness and between the trivial and non-trivial phases [38]. We generally observe good correspondence with the results of the linear stability analysis, Fig. 1. Namely, when the nonlinear Bloch wave is linearly stable the purity gap vanishes, as most wavevectors remain populated only by the initial random perturbations. On the other hand, instability allows the initial nonlinear Bloch wave to coherently populate other wavevectors, opening a purity gap. The purity gap also closes at $\Delta = \Delta_c = -(4J_2 + \Gamma I_0/2) \approx -2.2$ despite the nonlinear Bloch wave being unstable. This corresponds to closure of the band gap at $\boldsymbol{k} = (0, \pi)$. While the trivial and non-trivial phases exhibit a similar purity, their differing Chern numbers result in distinct polarization textures $\langle \hat{n}(\boldsymbol{k}) \rangle$, as illustrated in Fig.4(b,c). Thus, while the linear stability analysis is sensitive to the local band structure in the vicinity of the nonlinear Bloch wave, the long time instability dynamics are sensitive to the whole Brillouin zone and the band topology. This is our second important finding.

In conclusion, we have shown how the modulational instability of nonlinear Bloch waves is sensitive to the band topology. Notably, nonlinear wave mixing can populate an entire band, enabling the spontaneous creation of topologically non-trivial wave fields from simple plane wave initial states. Since the timescales involved appear to be shorter than the wave thermalization time, these effects should be experimentally observable using nonlinear waveguide arrays [6], Bose-Einstein condensates in optical lattices [21, 22], or exciton-polariton condensates [4, 5]. While we focused on the chiral-π-flux model, we have observed similar behaviour in other topological tight binding models, with lattices with a larger band flatness typically exhibiting emergence of a purity gap and well-defined Chern number for a wider range of nonlinearity strengths. It will be interesting to generalize our findings to Floquet systems such as the nonlinear waveguide array employed in Ref. [6], where perfectly flat topological bands have been demonstrated.

We thank Mikael Rechtsman for illuminating discussions. This research was supported by the Institute for Basic Science in Korea (IBS-R024-Y1, IBS-R024-D1) and the Australian Research Council Early Career Researcher Award (DE190100430).

[1] T. Ozawa et al., *Topological photonics*, Rev. Mod. Phys. **91**, 015006 (2019).

[2] D. Smirnova, D. Leykam, Y. D. Chong, and Y. Kivshar, *Nonlinear topological photonics*, Appl. Phys. Rev. **7**, 021306 (2020).

[3] A. Saxena, P. G. Kevrekidis, and J. Cuevas-Marave, *Nonlinearity and Topology*, Nonlinear Systems and Complexity **32**, 25 (2020).

[4] S. Klembt et al., *Exciton-polariton topological insulator*, Nature **562**, 552 (2018).

[5] F. Baboux et al., *Unstable and stable regimes of polariton condensation*, Optica **5**, 1163 (2018).

[6] S. Mukherjee and M. C. Rechtsman, *Observation of Floquet solitons in a topological bandgap*, Science **368**, 856 (2010).

[7] D. A. Smirnova et al., *Third-harmonic generation in photonic topological metasurfaces*, Phys. Rev. Lett. **123**, 103901 (2019).

[8] D. A. Dobrykh, A. V. Yulin, A. P. Slobozhanyuk, A. N. Poddubny, Y. S. Kivshar, *Nonlinear control of electromagnetic topological edge states*, Phys. Rev. Lett. **121**, 163901 (2018).

[9] S. Mittal, E. A. Goldschmidt, and M. Hafezi. *A topological source of quantum light*, Nature **561**, 502 (2018).

[10] M. J. Ablowitz, C. W. Curtis, and Y.-P. Ma, *Linear and nonlinear traveling edge waves in optical honeycomb lattices*, Phys. Rev. A **90**, 023813 (2014).

[11] Y. Lumer, M. C. Rechtsman, Y. Plotnik, and M. Segev, *Instability of bosonic topological edge states in the presence of interactions*, Phys. Rev. A **94**, 021801(R) (2016).

[12] Y. V. Kartashov and D. V. Skryabin, *Modulational instability and solitary waves in polariton topological insulators*, Optica **3**, 1228 (2016).

[13] D. Leykam and Y. D. Chong, *Edge Solitons in Nonlinear Photonic Topological Insulators*, Phys. Rev. Lett. **117**, 143901 (2016).

[14] Y. Lumer, Y. Plotnik, M. C. Rechtsman, and M. Segev, *Self-Localized States in Photonic Topological Insulators*, Phys. Rev. Lett. **111**, 243905 (2013).

[15] A. N. Poddubny and D. A. Smirnova, *Ring Dirac solitons in nonlinear topological systems*, Phys. Rev. A **98**, 013827 (2018).

[16] J. L. Marzuola, M. Rechtsman, B. Osting, and M. Bandres, *Bulk soliton dynamics in bosonic topological insulators*, arXiv:1904.10312.

[17] D. A. Smirnova, L. A. Smirnov, D. Leykam, and Y. S. Kivshar, *Topological edge states and gap solitons in the nonlinear Dirac model*, Laser Photon. Rev. **13**, 1900223 (2019).

[18] V. E. Zakharov and L. A. Ostrovsky, *Modulation instability: The beginning*, Physica D **238**, 540 (2009).

[19] R. W. Boyd, *Nonlinear Optics*, Academic Press, New York (2008).

[20] Y. S. Kivshar and M. Peyrard, *Modulational instabilities in discrete lattices*, Phys. Rev. A **46**, 3198 (1992).

[21] P. J. Everitt et al., *Observation of a modulational instability in Bose-Einstein condensates*, Phys. Rev. A **96**, 041601(R) (2017).

[22] J. H. V. Nguyen, D. Luo, and R. G. Hulet, *Formation of matter-wave soliton trains by modulational instability*, Science **356**, 422 (2017).

[23] Karlo Lelas, Ozana Čelan, David Prelogović, Hrvoje Buljan, and Dario Jukić, *Modulation instability in the nonlinear Schrödinger equation with a synthetic magnetic field: gauge matters*, arXiv:2003.12620.

[24] C.-E. Bardyn, S.D. Huber, and O. Zilberberg, *Measuring topological invariants in small photonic lattices*, New J. Phys. **16**, 123013 (2014).

[25] M. Aidelsburger, M. Lohse, C. Schweizer, M. Atala, J. T. Barreiro, S. Nascimbene, N. R. Cooper, I. Bloch, and N. Goldman, *Measuring the Chern number of Hofstadter bands with ultracold bosonic atoms*, Nature Phys. **11**, 162 (2015).

[26] M. Wimmer, H. M. Price, I. Carusotto, and U. Peschel, *Experimental measurement of the Berry curvature from anomalous transport*, Nature Phys. **13**, 545 (2017).

[27] M. Tarnowski, F. N. Ünal, N. Fläschner, B. S. Rem, A. Eckardt, K. Sengstock, and C. Weitenberg, *Measuring topology from dynamics from obtaining the Chern number from a linking number*, Nature Commun. **10**, 1728 (2019).

[28] A. V. Poshakinskiy, A. N. Poddubny, and M. Hafezi, *Phase spectroscopy of topological invariants in photonic crystals*, Phys. Rev. A **91**, 043830 (2015).

[29] W. Hu, J. C. Pillay, K. Wu, M. Pasek, P. P. Shum, and Y. D. Chong, *Measurement of a topological edge invariant in a microwave network*, Phys. Rev. X **5**, 011012 (2015).

[30] S. Mittal, S. Ganeshan, J. Fan, A. Vaezi, and M. Hafezi, *Measurement of topological invariants in a 2D photonic system*, Nature Photon. **10**, 180 (2016).

[31] P. Buonsante, R. Franzosi, and A. Smerzi, *Phase transitions at high energy vindicate negative microcanonical temperature*, Phys. Rev. E **95**, 052135 (2017).

[32] T. Mithun, Y. Kati, C. Danieli, and S. Flach, *Weakly Nonergodic Dynamics in the Gross-Pitaevskii Lattice*, Phys. Rev. Lett. **120**, 184101 (2018).

[33] M. Hafezi, P. Adhikari, and J. M. Taylor, *Chemical potential for light by parametric coupling*, Phys. Rev. B **92**, 174305 (2015).

[34] F. O. Wu, A. U. Hassan, and D. N. Christodoulides, *Thermodynamic theory of highly multimoded nonlinear optical systems*, Nature Photon. **13**, 776 (2019).

[35] T. Fösel, V. Peano, and F. Marquardt, *L lines, C points and Chern numbers: understanding band structure topology using polarization fields*, New J. Phys. **19**, 115013 (2017).

[36] D. Leykam and D. A. Smirnova, *Probing bulk topological invariants using leaky photonic lattices*, arXiv:2004.13215.

[37] R. W. Bomantara, W. Zhao, L. Zhou, and J. Gong, *Nonlinear Dirac cones*, Phys. Rev. B **96**, 121406(R) (2017).

[38] T. Neupert, L. Santos, C. Chamon, and C. Mudry, *Fractional Quantum Hall States at Zero Magnetic Field*, Phys. Rev. Lett. **106**, 236804 (2011).

[39] D. Träger et al., *Nonlinear Bloch modes in two-dimensional photonic lattices*, Opt. Exp. **14**, 1913 (2006).

[40] Y. V. Kartashov, B. A. Malomed, and L. Torner, *Solitons in nonlinear lattices*, Rev. Mod. Phys. **83**, 247 (2011).

[41] See Supplementary Material for further details.

[42] Alternatively, one could use a finite lattice superimposed with a sufficiently broad trapping potential.

[43] Y. Hu, P. Zoller, and J. C. Budich, *Dynamical Buildup of a Quantized Hall Response from Nontopological States*, Phys. Rev. Lett. **117**, 126803 (2016).

[44] C.-E. Bardyn, M. A. Baranov, C. V. Kraus, E. Rico, A.

Imamoglu, P. Zoller, and S. Diehl, *Topology by dissipation*, New J. Phys. **15**, 085001 (2013).

[45] J. C. Budich and S. Diehl, *Topology of density matrices*, Phys. Rev. B **91**, 154140 (2015).